Shape-coexisting rotation in neutron-deficient Hg and Pb nuclei

C. F. Jiao (焦长峰),[1] Yue Shi (石跃),[1] H. L. Liu (刘红亮),[2] F. R. Xu (许甫荣),[1,3,*] and P. M. Walker[4]
[1]*State Key Laboratory of Nuclear Physics and Technology, School of Physics, Peking University, Beijing 100871, China*
[2]*Department of Applied Physics, Xi'an Jiaotong University, Xi'an 710049, China*
[3]*State Key Laboratory of Theoretical Physics, Institute of Theoretical Physics, Chinese Academy of Sciences, Beijing 100190, China*
[4]*Department of Physics, University of Surrey, Guildford, Surrey GU2 7XH, United Kingdom*
(Received 17 November 2014; revised manuscript received 21 January 2015; published 9 March 2015)

For a shape-soft nucleus, the deformation change with increasing angular momentum of rotation can be significant. Total-Routhian-surface (TRS) calculations include the shape changes, but angular momentum is not conserved (neither is it a good quantum number, nor is it kept unchanged in the whole TRS mesh). In the projected shell model (PSM), the angular momentum appears as a good quantum number, but calculations have usually been performed with fixed deformation. In the present work, by performing angular-momentum projection on the mean-field potential-energy surface (PES), we can obtain an angular-momentum-conserved PES which gives deformation for a rotational state at a given spin. In order to investigate the shape-changing effect, we have chosen neutron-deficient Hg and Pb isotopes in which shape coexistence occurs. We interpret the irregular rotational behavior of the oblate bands at low spin as arising from deformation changes which are induced by collective rotation. At higher spin, the oblate rotational spectrum can also be influenced by the crossing between the $K = 0$ ground-state band and a low-K two-quasineutron band. Calculated g factors for the states of oblate bands are given for future experimental testing, and the intrinsic structures of high-K oblate states are investigated.

DOI: 10.1103/PhysRevC.91.034309 PACS number(s): 21.10.−k, 21.60.−n, 27.70.+q, 27.80.+w

I. INTRODUCTION

Nuclear shape is essential for determining various observables, such as moments of inertia, transitional quadrupole moments, and decay properties. The interdependence between shape and angular momentum has long been an interesting topic in nuclear physics. This arises from the shape coexistence, e.g., in neutron-deficient Hg and Pb nuclei [1–4]. For neutron-deficient Pb nuclei, it has been shown that the mean-field potential-energy surfaces (PES's) are dominated by sphericity, with two subminima located on prolate and oblate sides [5]. The two subminima are separated by a low potential barrier at triaxial deformation, which leads to mixing between the two shallow minima. Experimentally this mixing effect has been confirmed by the observation of $E0$ components in $J \rightarrow J$ transitions at low spins between bands built on different shapes in ^{188}Pb [6,7]. Due to the Coriolis force, the increase of angular momentum induces significant deformation changes for a shape-soft configuration. Although coexisting 0^+ states in light Hg and Pb nuclei have been studied extensively [5,8–11], the shape-changing effect remains unclear for high-spin states. Specifically, we seek to explain rotational bands based on oblate and prolate shapes, which have been observed in ^{184,186}Hg [12,13] and more recently in ^{186,188}Pb [7,14,15].

The shape coexistence or deformation change can be described by the total-Routhian-surface (TRS) calculation based on mean-field model [16,17]. However, the mean-field model and TRS method do not conserve a good angular momentum, while the TRS is calculated at a given frequency of collective rotation. For a soft nucleus, the calculation with a conserved angular momentum would be meaningful. To restore the broken rotational symmetry, the angular-momentum-projection (AMP) technique can be used. Hara and Sun developed a so-called projected shell model (PSM) [18,19] in which a deformed Nilsson basis is adopted and the angular momenta of model configurations are created by the AMP. The configurations are constructed in the quasiparticle (qp) scheme [18,19]. The existing PSM which we use considers zero-qp, two-qp, and four-qp configurations (for even-even nuclei) within three major Nilsson shells [18]. It has been shown that such PSM computation is fast and efficient [18,19]. However, the current PSM calculation is performed with a fixed deformation, and the result is dependent on what deformation is assumed. The choosing of the deformation parameter relies somewhat on data usually, which limits the predictive power of the model. In principle, if one takes a large enough model space with more multi-qp configurations and more Nilsson shells, the calculation should be less sensitive to the deformation parameter chosen.

AMP calculations for neutron-deficient even-mass Pb nuclei have also been done based on the Skyrme Hartree-Fock-BCS (HF-BCS) [20,21] or Gogny Hartree-Fock-Bogliubov (HFB) model [22]. In these calculations, however, the AMP was performed with only the qp vacuum, without considering excited qp configurations. The mixing of multi-qp configurations (K mixing) is important for the description of excited states [23]. It has been noted that the overestimated excitation energies in the calculations of Refs. [20–22] could be related to the absence of the K mixing in the wave functions [14,24].

The interplay between shape and qp excitation degrees of freedom should not be neglected. Multi-qp excitations can give rise to significant shape changes [25–27]. Also, shape fluctuations can strongly affect K mixing and hence the decay properties of states [28]. The projected shell model

*frxu@pku.edu.cn

(PSM) [18,19], as a calculation truncated in an angular-momentum-projected basis with qp configurations [29], is suitable for studying the behaviors of different qp states and mixing among them. However, the existing PSM applies to deformation-fixed calculations, i.e., assuming a fixed deformation in calculations. In principle, the shape-changing effect can be well included in the PSM by configuration mixing if the model space taken is large enough. For shape-soft light Hg and Pb isotopes, the shape-changing effect could be vital and needs to be addressed in the PSM calculations.

In the present paper, we investigate the rotational bands based on coexisting shapes by an angular-momentum-conserved PES calculation [30] which incorporates AMP into the macroscopic-microscopic (MM) model. Such a PES calculation treats both the shape-changing effect and multi-qp excitations in a self-consistent manner, which is expected to be important for the description of rotational states in a soft nucleus. Similar projected energy surface method has been suggested also by Tu and her coauthors, investigating a well-deformed nucleus, ^{172}W [31].

II. THE MODEL

The details of the PSM can be found in Refs. [18,32]. To avoid the spurious pairing collapse encountered in the BCS method which is used in the existing PSM, we have improved the pairing treatment by using the Lipkin-Nogami approach. As noticed, the inclusion of excited qp configurations is important. In the present calculation of even-even nuclei, the configurations considered include zero-qp, two-quasineutron, two-quasiproton, and four-qp (two quasineutrons plus two quasiprotons) components, i.e., $\{|\Phi_{\xi K}\rangle\} = \{|0\rangle, a^\dagger_{\nu_i} a^\dagger_{\nu_j}|0\rangle, a^\dagger_{\pi_i} a^\dagger_{\pi_j}|0\rangle, a^\dagger_{\nu_i} a^\dagger_{\nu_j} a^\dagger_{\pi_k} a^\dagger_{\pi_l}|0\rangle\}$, where $|0\rangle$ is the qp vacuum. The PSM many-body wave function can be expressed in terms of various projected configurations [18],

$$|\Psi^I\rangle = \sum_{\xi K} f^I_{\xi K} \hat{P}^I_{MK} |\Phi_{\xi K}\rangle, \tag{1}$$

where $\hat{P}^I_{MK}$ is the AMP operator. $|\Phi_{\xi K}\rangle$ denotes a mean-field configuration (before projection). An axially symmetric shape is assumed, and thus each basis state has a good quantum number of the spin projection K onto the symmetry axis. The coefficient $f^I_{\xi K}$ is the corresponding weight factor which is obtained by diagonalizing the eigenvalue equation,

$$\sum_{\xi' K'} \left(H^I_{\xi K \xi' K'} - E^I N^I_{\xi K \xi' K'}\right) f^I_{\xi' K'} = 0, \tag{2}$$

where $H^I_{\xi K \xi' K'}$ and $N^I_{\xi K \xi' K'}$ are the matrix elements of the Hamiltonian and the norm, respectively, defined by

$$H^I_{\xi K \xi' K'} = \langle \Phi_{\xi K} | \hat{H} \hat{P}^I_{K_\xi K'_{\xi'}} | \Phi_{\xi' K'} \rangle,$$
$$N^I_{\xi K \xi' K'} = \langle \Phi_{\xi K} | \hat{P}^I_{K_\xi K'_{\xi'}} | \Phi_{\xi' K'} \rangle. \tag{3}$$

The weight factor $f^I_{\xi K}$ reflects the mixing amplitudes of different qp configurations. The state $|\Psi^I\rangle$ is a linear superposition of various K states, i.e., K mixing is included.

The Hamiltonian takes the following form, which includes the quadrupole-quadrupole (QQ) interaction and the monopole plus quadrupole pairings [18]:

$$\hat{H} = \hat{H}_0 - \frac{\chi}{2} \sum_\mu \hat{Q}^\dagger_{2\mu} \hat{Q}_{2\mu} - G_M \hat{P}^\dagger \hat{P} - G_Q \sum_\mu \hat{P}^\dagger_{2\mu} \hat{P}_{2\mu}, \tag{4}$$

where $\hat{H}_0 = \sum_\alpha e_\alpha c^\dagger_\alpha c_\alpha$ with e_α for spherical Nilsson single-particle energies [18]. The monopole-pairing strength G_M is determined by the average gap method [33]. The quadrupole-pairing strength G_Q is taken to be proportional to G_M, with a constant factor of 0.24, i.e., $G_Q = 0.24 G_M$. We discuss the strength χ of the QQ interaction in more detail later.

In the PSM calculations, one usually needs a cutoff of the model space to reduce the computational task. The existing PSM considers three major Nilsson shells in calculations [18]. This means that the energy $\langle \Psi^I | \hat{H} | \Psi^I \rangle$ given by the PSM wave function $|\Psi^I\rangle$ in Eq. (1) is not the total energy of the nucleus but the energy of the valence particles. We can well assume that the angular momentum of an excited state is generated by the valence particles, but the total energy (not only the energy of valence particles) should be used in the determination of nuclear shape by minimizing the energy with respect to deformation. In the MM model, nuclear shape can be obtained by plotting the total energy surface. A similar method has also been adopted in the cranking shell model in which the total energy (in the body-fixed frame) of a rotational state is written as the total energy of the nucleus at rest and the energy change due to rotation [16,34]. Also, only the valence particles are taken into account in cranking calculations. Therefore, we can write the projected total energy for an excited state at spin I as

$$E^I(N,Z,\hat{\beta}) = E_{\rm MM}(N,Z,\hat{\beta}) + E^I_{\rm rot}(N,Z,\hat{\beta}), \tag{5}$$

where $\hat{\beta}$ represents a set of deformation parameters. $E_{\rm MM}(N,Z,\hat{\beta})$ is the total energy of the nucleus at rest, which can be calculated by the MM model including the macroscopic energy, the microscopic shell correction, and the pairing energy in the standard Strutinsky method. $E^I_{\rm rot}(N,Z,\hat{\beta})$ gives the energy gain due to rotation (including possible intrinsic excitation energy if the rotational state has, e.g., a broken-pair intrinsic structure), defined by

$$E^I_{\rm rot} = \frac{\langle \Psi^I | \hat{H} | \Psi^I \rangle}{\langle \Psi^I | \Psi^I \rangle} - \frac{\langle 0 | \hat{H} | 0 \rangle}{\langle 0 | 0 \rangle}. \tag{6}$$

The first term is the energy of the valence-particle system at spin I, which is calculated by the projected wave function $|\Psi^I\rangle$. The second term is the energy of the valence-particle system before AMP, which is calculated by the unprojected qp vacuum $|0\rangle$. Note that the energy $E^I_{\rm rot}$ is not equal to zero even for the $I = 0$ ground state of even-even nucleus. For ground-state case, it is in fact an energy correction due to the restoration of the rotational symmetry. This energy correction can be sensitive to deformation and therefore would play a significant role in the determination of the shape of a soft nucleus, even for the ground state.

We should point out that the energy calculations by $\langle \Psi^I | \hat{H} | \Psi^I \rangle$ and $\langle 0 | \hat{H} | 0 \rangle$ in Eq. (6) have the double-counting

problem. This is because the PSM uses the Hamiltonian [see Eq. (4)] in which the energy (except the QQ and residual pairing interactions) is written as a simple summation of one-body Nilsson single-particle energies. Though the double-counting effect should be largely canceled due to calculating the energy difference at spins I and zero in Eq. (6), it is not removed completely. Therefore, Eq. (6) gives an approximation of the energy change due to rotational excitation. The deformation-fixed PSM has the same problem. This situation appears also in the TRS method, where the energy change due to rotation is given by $\langle\Psi^\omega|\hat{H}^\omega|\Psi^\omega\rangle - \langle\Psi^\omega|\hat{H}^\omega|\Psi^\omega\rangle^{\omega=0}$ with the deformed Nilsson or Woods-Saxon potentials used [16,17,35]. The double-counting problem is not encountered in modeling based on the HF or HFB approximation with a microscopic two-body interaction (e.g., Skyrme or Gogny force), in which the Hamiltonian of the many-body nucleus is not simply written as a summation of one-body plus residual two-body pairing terms. For example, the recent works by Bally *et al.* [36] and by Satuła *et al.* [37] applied angular-momentum and particle-number (or isospin) projections to no-core calculations based on the Skyrme HF or HFB approximation, in which the double-counting problem does not appear.

In the present calculations, the macroscopic energy is calculated by the new version of the liquid-drop model (called "new" liquid drop (NLD) in Ref. [38]) with the inclusion of a Gauss-curvature term, which takes the following form [38]:

$$\begin{aligned} E_{\rm mac}(N,Z,\hat{\beta}) &= b_{\rm vol}(1-\kappa_{\rm vol}\mathcal{I}^2)A + b_{\rm surf}(1-\kappa_{\rm surf}\mathcal{I}^2) \\ &\quad\times A^{2/3}B_{\rm surf}(\hat{\beta}) + b_{\rm curG}(1-\kappa_{\rm curG}\mathcal{I}^2)A^0 \\ &\quad+\frac{3}{5}e^2\frac{Z^2}{r_0^{ch}A^{1/3}}B_{\rm Coul}(\hat{\beta}) - C_4\frac{Z^2}{A} + E_{\rm W}, \end{aligned} \quad (7)$$

where $\mathcal{I}=(N-Z)/A$. $b_{\rm vol}$, $\kappa_{\rm vol}$, $b_{\rm surf}$, $\kappa_{\rm surf}$ $b_{\rm curG}$, $\kappa_{\rm curG}$, r_0^{ch}, and C_4 are the liquid-drop model parameters. The Wigner term $E_{\rm W}$ is given as $E_{\rm W}=-10e^{-4.2|\mathcal{I}|}$ according to Refs. [38,39].

The original values of the parameters in the liquid-drop model were determined by calculating binding energies and fitting data, without considering explicitly the rotational symmetry. The effect from the restoration of the symmetry exists even in the spin-zero ground state as mentioned above. Therefore, we calibrate the NLD parameters by refitting binding energies, including the effect from restoring the rotational symmetry. In our previous paper [30], we have given a detailed explanation of the parameter readjustment, where we selected 150 nuclei covering the regions with masses of ∼60, 180, and 240. The refitted result give a root-mean-square deviation of 0.725 MeV for binding energies between calculations and data [30] for the 150 nuclei. Also, the readjusted parameters have led to the better results of fission barriers, compared to experiments and other model calculations [30].

The PES is calculated in the (β_2,β_4) deformation space. In the deformation-fixed PSM calculations, the QQ interaction strength χ is determined by the assumption that the PSM Hamiltonian gives the same QQ interaction as that derived from the Nilsson model [18]. In the present calculations, we obtain a χ value at each deformation point of the $(\beta_2,\ \beta_4)$ lattice using the method above. At the same time we can obtain the PES of the ground state, which is analyzed for the determination of the χ parameter. Note that the χ value thus obtained can change slightly with changing deformation in the PES lattice. We assume that the χ value obtained at the ground-state PES minimum should be the most reasonable value. With such a χ value, we perform the deformation-variable PSM calculations, obtaining the projected PES for each given angular momentum. The excitation energy and deformation at a given spin are obtained by minimizing the corresponding projected PES. Several different PES's at the same spin I may be obtained, corresponding to different intrinsic configurations.

The g factor which reflects the magnetic properties of a state is a sensitive probe of the multi-qp structure. It is defined by

$$g(I) = g_\nu(I) + g_\pi(I), \quad (8)$$

with $g_\tau(I)$ (π for protons and ν for neutrons) given by

$$\begin{aligned} g_\tau(I) = \frac{1}{\mu_N\sqrt{I(I+1)}}\big[&g_l^\tau\langle\Psi^I||\hat{j}^\tau||\Psi^I\rangle \\ &+\left(g_s^\tau-g_l^\tau\right)\langle\Psi^I||\hat{s}^\tau||\Psi^I\rangle\big], \end{aligned} \quad (9)$$

where $|\Psi^I\rangle$ is the wave function of Eq. (1). In the present work, we use the standard values for g_l and g_s (i.e., $g_l^\pi=1$, $g_l^\nu=0$, $g_s^\pi=5.586\times0.75$, and $g_s^\nu=-3.826\times0.75$). g_s^π and g_s^ν are both reduced by a quenching factor of 0.75 from the free-nucleon values to account for the core-polarization and meson-exchange current corrections [40].

In principle, one can use the particle representation to construct the model configurations and truncate the model space by making, e.g., a configuration energy cutoff, which is similar to usual shell-model calculations. However, the existing PSM takes a simple phenomenological Hamiltonian in which the residual two-body force is written as the pairing interaction. In this case, the paired qp representation should be more effective to give the important configurations. It is understood naturally that the qp-vacuum, two-qp, and four-qp configurations construct the most important configurations for the low-energy states of even-even nuclei. The model space is also dramatically dependent on how many shells are taken. In the existing PSM, three harmonic oscillator (HO) shells are taken. The limit on the numbers of qp configurations and HO shells is to reduce the dimension of the model. However, a too small model space would give unstable results against the dimension or other parameters. It is found that the deformation-fixed PSM calculation is sensitive to the deformation parameter assumed. In principle, the calculation should be insensitive to the deformation parameter if a large enough model space is taken. The deformation-changing effect can be included by sufficient configuration mixing. We have not verified the stability of the model itself against the model space, but assume that this problem has been well tested previously by the authors of the existing PSM [18,19]. In the present work, we develop a projected PES to give the optimal deformation (which can be variable with angular momentum) for the model-space-limited PSM calculation.

III. CALCULATIONS AND DISCUSSIONS

Among neutron-deficient Hg and Pb isotopes in which shape coexistence happens, ^{184,186}Hg and ^{186,188}Pb are of particular interest. Owing to the fact that both prolate and oblate rotational bands have been observed in these nuclei, they provide an excellent testing ground for the shape-changing effect. In the classic picture, if the shape of an object keeps unchanged, the rotational spectrum should obey the regular $I(I+1)$ pattern. However, it was observed that in ^{184,186}Hg and ^{186}Pb, the oblate levels are compressed when compared to the regular $I(I+1)$ pattern [12–14]. Whether the origin of the irregular behavior involves significant shape change remains an open question [14].

The present projected PES calculations are restricted to positive-parity states and axial symmetry. We have performed such PES calculations for light even-even Hg and Pb nuclei, with particular attention to ^{184,186}Hg and ^{186,188}Pb. Figure 1 plots the projected PES's for ^{186}Hg against the β_2 deformation. It is seen that the ground-state calculation without AMP gives a soft shape (i.e., a relatively flat potential energy curve), while the projection significantly enhances the depths of the minima appearing at both prolate and oblate deformations. Figure 1 also shows the calculated excited states. One can see that the shape changes with increasing spin. In Fig. 2, we plot the calculated spectra of prolate bands in light Hg and Pb nuclei. The calculated energies are in good agreement with experimental data.

To understand the anomaly in oblate bands, we have carried out various calculations and compared with experimental data for ^{186}Hg as a detailed example, shown in Fig. 3. It can be seen that the calculation with fixed deformation and no multi-qp mixing [Fig. 3(a)] overestimates remarkably the energies of the experimental states. If we allow deformation to change with spin (i.e., the deformation is determined self-consistently by minimizing the projected PES), the calculation is improved significantly [Fig. 3(b)] though no multi-qp mixing is considered. However, the 8^+ level is still significantly higher than the observed energy. The calculation with considering both shape change and multi-qp mixing (K mixing) reproduces well the experimental spectrum [Fig. 3(c)]. For the 2^+, 4^+, and 6^+ levels of the oblate band, the comparison between calculations without and with multi-qp mixing tells us that the multi-qp excitation contribution to the irregularity is small.

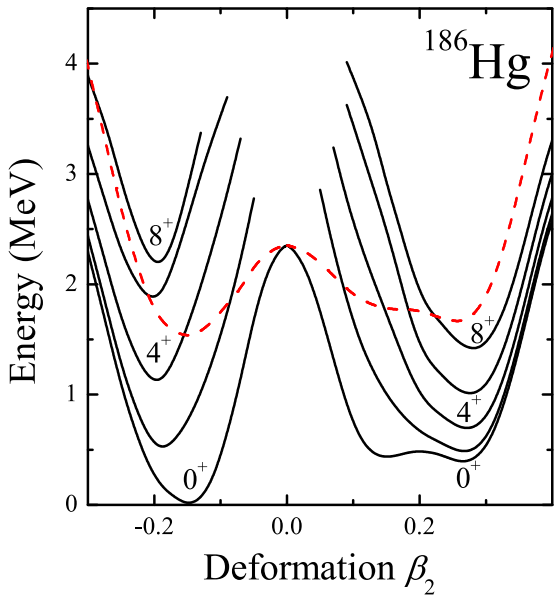

FIG. 1. (Color online) Calculated angular-momentum-conserved PES's for ^{186}Hg at different spins. At each β_2 value, the energy has been minimized with respect to the β_4 deformation. The dashed line indicates the ground-state energy curve without AMP.

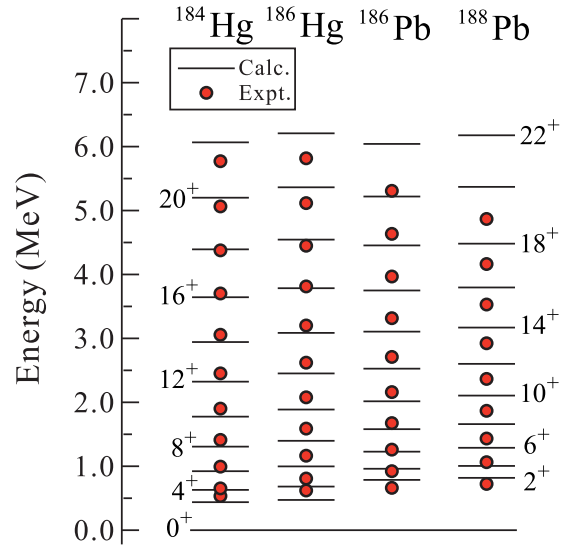

FIG. 2. (Color online) Comparison between calculated and experimental lowest-energy prolate bands in ^{184,186}Hg and ^{186,188}Pb. Experimental data are taken from Refs. [7,12–14].

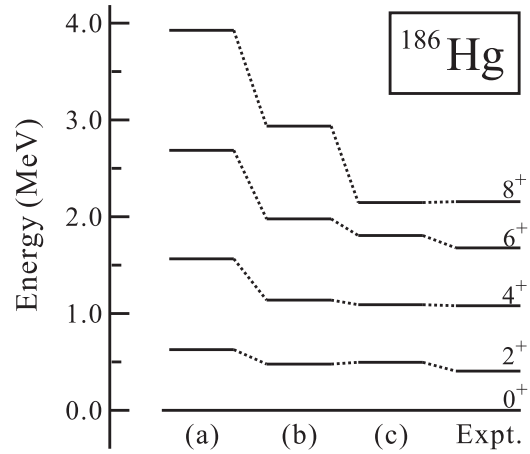

FIG. 3. Comparison between calculated and experimental spectra of the oblate band in ^{186}Hg: (a) calculation with fixed deformation at the ground state ($\beta_2 = -0.15$, $\beta_4 = -0.01$) and no multi-qp admixture; (b) calculation without multi-qp admixture but considering self-consistent deformation change (i.e., deformation determined self-consistently by minimizing the projected PES); (c) calculation with the inclusion of both shape change and multi-qp admixtures. Experimental data are taken from Ref. [13].

Figure 1 shows that the oblate deformation increases from $|\beta_2| = 0.15$ to 0.20 when spin increases from $I = 0\hbar$ to $6\hbar$. Therefore, the irregularity for the oblate 2^+, 4^+, and 6^+ levels should be mainly attributed to the deformation change induced by collective rotation.

As discussed above, the multi-qp admixture plays an important role in the description of the oblate 8^+ state in Fig. 3. The calculated PSM wave functions show that the lowest oblate 8^+ states in $^{178-186}$Hg and $^{186-194}$Pb are dominated by the $K^\pi = 8^+$, $\pi 9/2^-[505] \otimes \pi 7/2^-[514]$ configuration, meaning that oblate multi-qp excitations become significant at $I \geqslant 8\hbar$. This has been supported by the observation of the $K^\pi = 8^+$ isomers in even-even $^{190-196}$Pb [4], and the configuration is supported further by g-factor measurements in the neighboring nuclei ^{198,200}Po [41]. At oblate shape, high-Ω $\pi h_{9/2}$ orbits appear near the proton Fermi surfaces of $Z = 80$ and 82, which leads to the two-quasiproton $K^\pi = 8^+$ state being more favored energetically than the collective oblate 8^+ state. The behavior of oblate states at spin $I \geqslant 8\hbar$ can be influenced significantly by multi-qp components.

A low-K rotation-aligned band (known as s band) can cross with the 0-qp ground-state band (g band) and become yrast. However, when the Fermi surface lies in the middle of the $\nu i_{13/2}$ orbits, bands with high-K configurations (known as t bands) may compete with the g and/or s band [42–44]. To illustrate the rotational behavior of each multi-qp configuration as well as its relative energy compared to other components, we can plot rotational bands built on different multi-qp configurations without K mixing in one figure, i.e., a band diagram [18]. The band diagram for a given qp configuration is given by [18]

$$E^I_{\xi K} = \frac{\langle \Phi_{\xi K} | \hat{H} \hat{P}^I_{K_\xi K_\xi} | \Phi_{\xi K} \rangle}{\langle \Phi_{\xi K} | \hat{P}^I_{K_\xi K_\xi} | \Phi_{\xi K} \rangle}, \tag{10}$$

where $|\Phi_{\xi K}\rangle$ is a qp configuration [cf. Eq. (1)].

Figure 4 displays the low-lying oblate band diagram for ^{186}Hg. For simplicity, we only plot the most important configurations. Our calculation shows that the two-quasiproton $K^\pi = 8^+$, $\pi 9/2^-[505] \otimes \pi 7/2^-[514]$ band is lower than the $K = 0\, g$ band. The two-quasineutron $K^\pi = 1^+$, $\nu 9/2^+[624] \otimes \nu 7/2^+[633]$ band shows a typical aligned behavior of the s band, crossing with the g band at $I \approx 8\hbar$ and again with the two-quasiproton $K^\pi = 8^+$ band at $I \approx 10\hbar$. It is seen that the two-quasineutron $K^\pi = 8^+$ band with the $\nu 9/2^+[624] \otimes \nu 7/2^+[633]$ configuration crosses with the $K^\pi = 8^+$ two-quasiproton band at $I \approx 12\hbar$. This is because the $\nu 9/2^+[624]$ and $\nu 7/2^+[633]$ orbits from the $\nu i_{13/2}$ shell have large angular-momentum projections on both the deformation axis and the collective rotation axis, which would lead to Fermi alignment (i.e., alignment to an axis intermediate between the deformation axis and the collective rotation axis) [45]. The Fermi alignment lowers the energy of two-quasiproton $K^\pi = 8^+\, t$ band and hence results in competition between the s band and the t band, which is similar to the t-band crossing observed in ^{180}W [43]. At higher spins, a four-qp $K^\pi = 16^+$ ($\nu 9/2^+[624] \otimes \nu 7/2^+[633] \otimes \pi 9/2^-[505] \otimes \pi 7/2^-[514]$) configuration is predicted to form the lowest oblate 16^+ states in $^{184-188}$Hg and $^{186-190}$Pb.

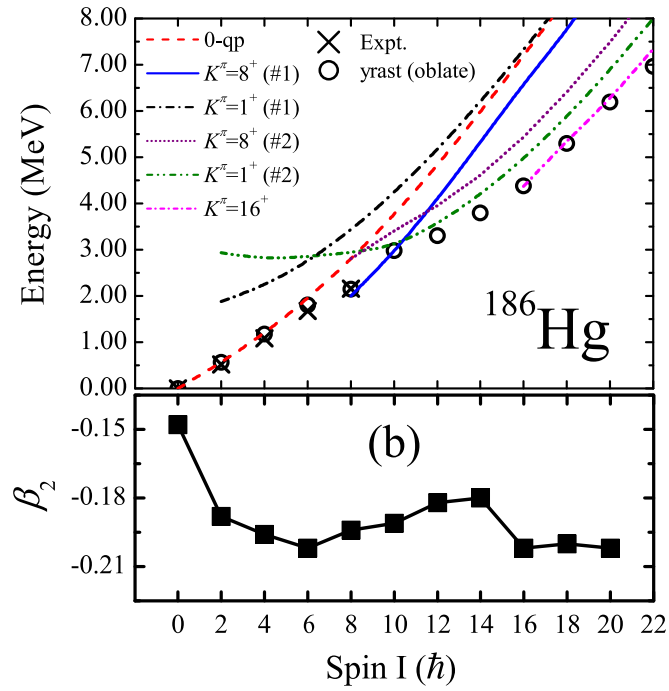

FIG. 4. (Color online) Calculated band diagrams and β_2 deformations of the oblate states for ^{186}Hg. The $K^\pi = 8^+$(#1) and $K^\pi = 1^+$(#1) bands are based on the $\pi 9/2^-[505] \otimes \pi 7/2^-[514]$ configuration. The $K^\pi = 8^+$(#2) and $K^\pi = 1^+$(#2) bands are based on the $\nu 9/2^+[624] \otimes \nu 7/2^+[633]$ configuration. The $K^\pi = 16^+$ band is based on the $\nu 9/2^+[624] \otimes \nu 7/2^+[633] \otimes \pi 9/2^-[505] \otimes \pi 7/2^-[514]$ configuration. The "yrast (oblate)" band denotes the lowest oblate states with K mixing.

This is because the neutron Fermi surfaces of $104 \leqslant N \leqslant 108$ are near the $\nu 9/2^+[624]$ and $\nu 7/2^+[633]$ orbits. Also, Fig. 4 gives a clear example of significant shape changes which are induced by multi-qp excitations. The β_2 value changes drastically after the crossing of bands with different intrinsic structures.

A 16^+ isomer with a half-life of 20 ns was observed in ^{190}Pb [46]. Its configuration remains unclear. The experimental 16^+ isomer decays to the oblate two-quasiproton $K^\pi = 11^-$ band rather than to the $(\nu i_{13/2})^{-4}$ multiplets which feed the nearly spherical 12^+ isomer. This suggests that the 16^+ isomer observed in ^{190}Pb is unlikely to be a nearly spherical seniority-four multiplet [46]. Instead, we propose it as a candidate for the predicted oblate $K^\pi = 16^+$ state with a two-proton–two-neutron configuration. Table I lists the detailed results for the oblate $K^\pi = 8^+$ and $K^\pi = 16^+$ states, compared with available experimental energies of the levels that are assigned as oblate 8^+ and 16^+ states [7,12–14,46,48]. Our calculations reproduce well experimental values. Also, our obtained deformations of the oblate $K^\pi = 8^+$ states are in good agreement with configuration-constrained PES calculations which give slightly higher energies (by 250–400 keV) [47]. We have explored the single-particle energies given by the Woods-Saxon potential employed in the configuration-constrained PES calculations [47] and the Nilsson potential used in the present work. It is found that, at $\beta_2 \approx -0.18$, the energy

TABLE I. Calculated deformations, g factors, and excitation energies $E_{\text{cal.}}$ (in keV) for the oblate $K^\pi = 8^+$ ($\pi 9/2^-[505] \otimes \pi 7/2^-[514]$) and $K^\pi = 16^+$ ($\nu 9/2^+[624] \otimes \nu 7/2^+[633] \otimes \pi 9/2^-[505] \otimes \pi 7/2^-[514]$) states in neutron-deficient Hg and Pb isotopes. Experimental data are taken from Refs. [7,12–14,46,48].

Nuclei	K^π	β_2	β_4	g factor	$E_{\text{cal.}}$	$E_{\text{exp.}}$
^{178}Hg	8^+	−0.19	0.008	0.930	2612	
^{180}Hg	8^+	−0.19	0.007	0.928	2009	
^{182}Hg	8^+	−0.19	0.004	0.926	2291	
^{184}Hg	8^+	−0.19	0.001	0.927	2227	2057
	16^+	−0.20	0.005	0.352	4887	
^{186}Hg	8^+	−0.19	−0.003	0.869	2147	2156
	16^+	−0.20	0.005	0.341	4381	
^{186}Pb	8^+	−0.18	0.013	0.873	2205	2162
	16^+	−0.19	0.014	0.341	4539	
^{188}Pb	8^+	−0.18	0.009	0.873	2094	2299
	16^+	−0.19	0.010	0.341	4325	
^{190}Pb	8^+	−0.18	0.002	0.874	2116	2252
	16^+	−0.19	0.004	0.342	4420	4517
^{192}Pb	8^+	−0.18	−0.005	0.875	2251	2304
^{194}Pb	8^+	−0.17	−0.009	0.890	2473	2438

difference between the $\pi 9/2^-[505]$ and $\pi 7/2^-[514]$ orbits obtained with the Woods-Saxon potential is about 300 keV larger than that given by the Nilsson potential, which gives rise to the higher calculated energies of the oblate $K^\pi = 8^+$ states in Ref. [47]. For the oblate two-quasiproton $K^\pi = 8^+$ states, the calculated g-factor values are about 0.9. We use $g = g_R + (g_K - g_R) \cdot \frac{K^2}{I(I+1)}$ and assume $g_R = 0.28$ [49] to obtain $|g_K - g_R| \approx 0.7$ for the $K^\pi = 8^+$ states. This large $|g_K - g_R|$ value indicates that the $M1$ cascade transitions are more favored than the $E2$ crossover transitions within the $K^\pi = 8^+$ band, which is compatible with the observation in ^{192}Pb [50].

Experimentally, rotational bands associated with oblate shapes have been extended to spin $I > 10\hbar$ in ^{186}Pb [14,15] and ^{188}Pb [6,7], which opens up the possibility to investigate the predicted bandcrossing between the g band and the two-quasineutron s band. Figure 5 shows the rotational energies (relative to an arbitrary rigid rotor) of the oblate bands in ^{186,188}Pb. For ^{188}Pb, the calculated oblate g band and two-quasineutron s band give a good description of the observed oblate levels. The downward trend starting from $I \approx 10\hbar$ in experimental energies can be attributed to the bandcrossing with the two-quasineutron oblate band. For ^{186}Pb, the behavior of the oblate levels is similar. The present calculations overestimate the excitation energies of the oblate states in ^{186}Pb. Nevertheless, the calculated trend of energies is in accord with the observation, and the discrepancy could be an indication of strong mixing between the g-band and s-band configurations which is not fully incorporated in the present calculation.

A crucial test for the predicted bandcrossing is to measure the g factors of the states before and after crossing. As the states have different structures, their g factors would give clear indications. Figure 6 shows the calculated g factors for

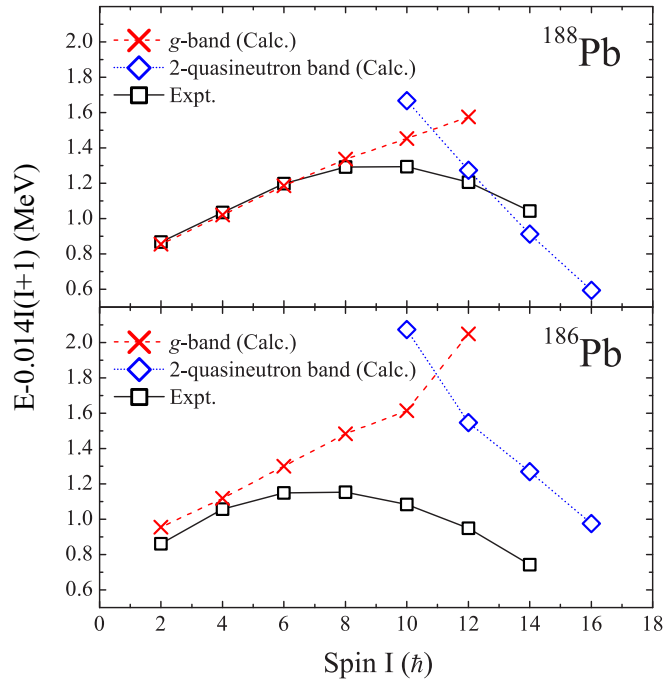

FIG. 5. (Color online) Energies (relative to an arbitrary rigid rotor) for oblate bands in ^{186,188}Pb. Experimental data are taken from Refs. [7,14].

the oblate bands in ^{188}Pb and ^{186}Pb, with decomposition of the total g factor into proton and neutron contributions. Both contributions show a reduction at spin $I = 12\hbar$, which makes the total g factor fall to about zero. This sudden change is due to the two-quasineutron band crossing with the g band. Further measurements of g factors for oblate states are needed.

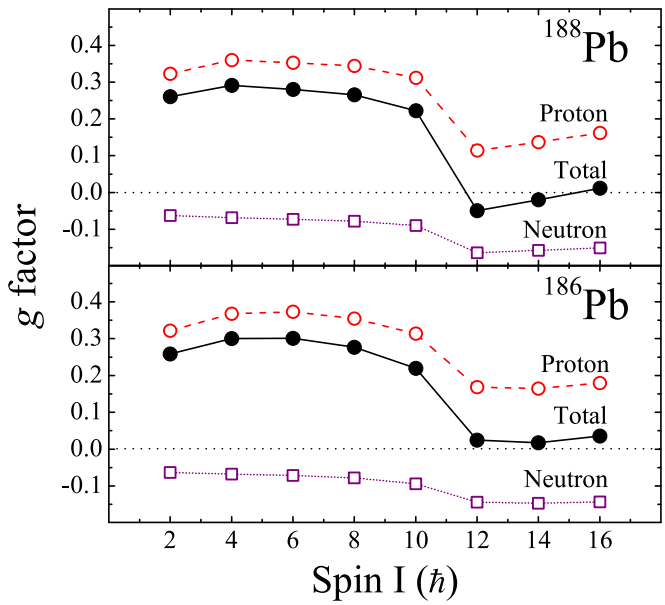

FIG. 6. (Color online) Calculated g factors for the oblate bands in ^{186,188}Pb, with decomposition of the total g factor (dots) into proton (circles) and neutron (squares) contributions.

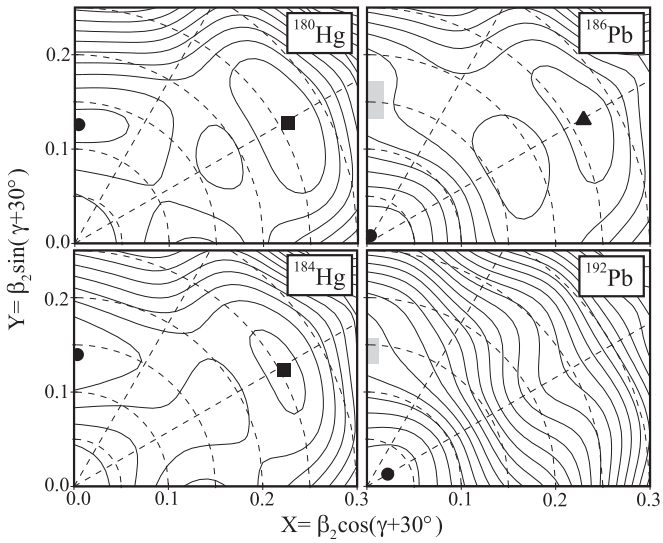

FIG. 7. Mean-field PES's for the ground states of ^{180,184}Hg and ^{186,192}Pb calculated with the nonaxial deformed Woods-Saxon potential. The energy difference between neighboring contours is 200 keV. The solid circles, squares, and triangles denote the first, second, and third lowest minima, respectively. A low-lying flat region at oblate shape ($\gamma = 60^\circ$) is indicated by shading.

It provides not only a testing of our prediction but also direct information about the role of the $\nu i_{13/2}$ orbits in the very neutron-deficient region.

The present projected PES calculations are limited to axially symmetric shapes. However, the shallow prolate and oblate minima given by such calculations may become triaxially deformed with inclusion of the γ degree of freedom. Figure 7 displays the mean-field PES's calculated in the (β_2,γ,β_4) deformation space with the nonaxial deformed Woods-Saxon potential for neutron-deficient Hg and Pb isotopes. It can be seen that no minimum appears for triaxial shapes in the ground-state PES's for the investigated Hg and Pb isotopes. Therefore, it is justified for us to limit the angular-momentum-conserved PES calculations to the (β_2,β_4) deformation space in this work. Nevertheless, it would be interesting to explore the combined effect from both K mixing and prolate-oblate shape mixing in future work.

IV. SUMMARY

Investigation of shape-coexisting rotational states in $^{178-186}$Hg and $^{186-194}$Pb has been carried out by using angular-momentum-conserved potential-energy-surface calculations which incorporate the AMP into the macroscopic-microscopic model. It is found that both shape-changing effects and multi-qp excitations are essential for the description of rotational states in the shape-soft neutron-deficient Hg and Pb isotopes. The irregular rotational behavior of the oblate states at low spins is interpreted as arising from shape changes which are induced by collective rotation. At higher spins, the rotational spectrum is strongly influenced by the bandcrossing between the $K = 0$ ground-state band and a two-quasineutron low-K band. We have calculated g factors for future experiments to test our predictions. Also, the intrinsic structures of oblate $K^\pi = 8^+$ and $K^\pi = 16^+$ states are investigated, combined with an analysis of their g factors.

ACKNOWLEDGMENTS

We thank Y. Sun for providing the code of the PSM. Valuable comments from R. Wyss, P. Ring, W. Nazarewicz, Y. S. Chen, Z. C. Gao, Y. L. Ye, and D. X. Jiang are acknowledged. This work has been supported by the National Key Basic Research Program of China under Grant No. 2013CB83440; the National Natural Science Foundation of China under Grants No. 11235001, No. 11320101004, and No. 11205120; the Open Project Program of State Key Laboratory of Theoretical Physics, Institute of Theoretical Physics, Chinese Academy of Sciences, China (No.Y4KF041CJ1); and the UK Science and Technology Facilities Council under Grant No. ST/J000051/1.

[1] K. Heyde and J. L. Wood, Rev. Mod. Phys. **83**, 1467 (2011).
[2] A. N. Andreyev *et al.*, Nature (London) **405**, 430 (2000).
[3] J. L. Wood, K. Heyde, W. Nazarewicz, M. Huyse, and P. Van Duppen, Phys. Rep. **215**, 101 (1992).
[4] R. Julin, K. Helariutta, and M. Muikku, J. Phys. G **27**, R109 (2001).
[5] R. Bengtsson and W. Nazarewicz, Z. Phys. A **334**, 269 (1989).
[6] G. D. Dracoulis, G. J. Lane, A. P. Byrne, A. M. Baxter, T. Kibédi, A. O. Macchiavèlli, P. Fallon, and R. M. Clark, Phys. Rev. C **67**, 051301(R) (2003).
[7] G. D. Dracoulis, G. J. Lane, A. P. Byrne, T. Kibédi, A. M. Baxter, A. O. Macchiavèlli, P. Fallon, and R. M. Clark, Phys. Rev. C **69**, 054318 (2004).
[8] R. Bengtsson, T. Bengtsson, J. Dudek, G. Leander, W. Nazarewicz, and J.-Y. Zhang, Phys. Lett. B **183**, 1 (1987).
[9] W. Nazarewicz, Phys. Lett. B **305**, 195 (1993).
[10] R. R. Chasman, J. L. Egido, and L. M. Robledo, Phys. Lett. B **513**, 325 (2001).
[11] T. Niksic, D. Vretenar, P. Ring, and G. A. Lalazissis, Phys. Rev. C **65**, 054320 (2002).
[12] J. K. Deng *et al.*, Phys. Rev. C **52**, 595 (1995).
[13] W. C. Ma *et al.*, Phys. Rev. C **47**, R5 (1993).
[14] J. Pakarinen *et al.*, Phys. Rev. C **75**, 014302 (2007).
[15] J. Pakarinen *et al.*, Phys. Rev. C **72**, 011304(R) (2005).
[16] W. Nazarewicz, J. Dudek, R. Bengtsson, T. Bengtsson, and I. Ragnarsson, Nucl. Phys. A **435**, 397 (1985).
[17] W. Satuła, R. Wyss, and P. Magierski, Nucl. Phys. A **578**, 45 (1994).
[18] K. Hara and Y. Sun, Int. J. Mod. Phys. E **04**, 637 (1995).
[19] Y. Sun, J.-Y. Zhang, and M. Guidry, Phys. Rev. Lett. **78**, 2321 (1997).
[20] T. Duguet, M. Bender, P. Bonche, and P.-H. Heenen, Phys. Lett. B **559**, 201 (2003).

[21] M. Bender, P. Bonche, T. Duguet, and P.-H. Heenen, Phys. Rev. C **69**, 064303 (2004).
[22] R. R. Rodríguez-Guzmán, J. L. Egido, and L. M. Robledo, Phys. Rev. C **69**, 054319 (2004).
[23] Y. Sun, X. R. Zhou, G. L. Long, E. G. Zhao, and P. M. Walker, Phys. Lett. B **589**, 83 (2004).
[24] P. Rahkila *et al.*, Phys. Rev. C **82**, 011303(R) (2010).
[25] F. R. Xu, P. M. Walker, J. A. Sheikh, and R. Wyss, Phys. Lett. B **435**, 257 (1998).
[26] F. R. Xu, P. M. Walker, and R. Wyss, Phys. Rev. C **59**, 731 (1999).
[27] P. M. Walker and F. R. Xu, Phys. Lett. B **635**, 286 (2006).
[28] P. M. Walker and G. D. Dracoulis, Hyperfine Interact. **135**, 83 (2001).
[29] L. J. Wang, F. Q. Chen, T. Mizusaki, M. Oi, and Y. Sun, Phys. Rev. C **90**, 011303(R) (2014).
[30] C. F. Jiao, J. C. Pei, and F. R. Xu, Phys. Rev. C **90**, 054314 (2014).
[31] Y. Tu, Y. S. Chen, Z. C. Gao, S. Y. Yu, and L. Liu, Sci. China Phys. Mech. Astron. **57**, 2054 (2014).
[32] G. X. Dong, X. B. Wang, H. L. Liu, and F. R. Xu, Phys. Rev. C **88**, 024328 (2013).
[33] P. Möller and J. R. Nix, Nucl. Phys. A **536**, 20 (1992).
[34] R. Wyss, W. Satuła, W. Nazarewicz, and A. Johnson, Nucl. Phys. A **511**, 324 (1990).
[35] F. R. Xu, W. Satula, and R. Wyss, Nucl. Phys. A **669**, 119 (2000).
[36] B. Bally, B. Avez, M. Bender, and P.-H. Heenen, Phys. Rev. Lett. **113**, 162501 (2014).
[37] W. Satuła, J. Dobaczewski, and M. Konieczka, arXiv:1408.4982v1 [nucl-th].
[38] K. Pomorski and J. Dudek, Phys. Rev. C **67**, 044316 (2003).
[39] W. D. Myers and W. J. Swiatecki, Nucl. Phys. **81**, 1 (1966).
[40] B. Castel and I. S. Towner, *Modern Theories of Nuclear Moments* (Clarendon Press, Oxford, 1990).
[41] A. Maj, H. Grawe, H. Kluge, A. Kuhnert, K. H. Maier, J. Recht, N. Roy, H. Hübel, and M. Guttormsen, Nucl. Phys. A **509**, 413 (1990).
[42] P. M. Walker, G. D. Dracoulis, A. P. Byrne, B. Fabricius, T. Kibédi, and A. E. Stuchbery, Phys. Rev. Lett. **67**, 433 (1991).
[43] P. M. Walker, K. C. Yeung, G. D. Dracoulis, P. H. Regan, G. J. Lane, P. M. Davidson, and A. E. Stuchbery, Phys. Lett. B **309**, 17 (1993).
[44] C. J. Pearson *et al.*, Phys. Rev. Lett. **79**, 605 (1997).
[45] S. Frauendorf, Phys. Scr. T **4**, 349 (1983).
[46] G. D. Dracoulis, A. P. Byrne, and A. M. Baxter, Phys. Lett. B **432**, 37 (1998).
[47] Y. Shi, F. R. Xu, H. L. Liu, and P. M. Walker, Phys. Rev. C **82**, 044314 (2010).
[48] M. Ionescu-Bujor *et al.*, Phys. Lett. B **650**, 141 (2007).
[49] M. Ionescu-Bujor *et al.*, Phys. Rev. C **81**, 024323 (2010).
[50] A. N. Wilson *et al.*, Eur. Phys. J. A **43**, 145 (2010).